DALLEY, N. K., MUELLER, N. H. & SIMONSEN, S. H. (1972). *Inorg. Chem.* **11**, 1840–1845.
DURSKI, Z. (1978). *Acta Cryst.* A**34**, S94.
FERRARIS, G. & FRANCHINI-ANGELA, M. (1972). *Acta Cryst.* B**28**, 3572–3583.
GENTILE, P. S., WHITE, J. & HADDAD, S. (1974). *Inorg. Chim. Acta*, **8**, 97–103.
GIESEN, W. VAN DE & STAM, C. H. (1972). *Cryst. Struct. Commun.* **1**, 257–260.
GOŁĘBIEWSKI, A. (1978). Private communication.
IVANOV, V. I. & SIMONOV, YU. A. (1976). *Kristalokhimia Nieorganicheskikh Soiedinienii*, edited by T. MALINOWSKI, pp. 72–113. Kishiniev: Shtiinca.
KARLE, I. L. (1975). *Peptides: Chemistry, Structure and Biology*, edited by R. WALTER & J. MEINHOFER, pp. 61–84. Michigan: Ann Arbor.
KURKUTOVA, E. N. & RAU, T. F. (1972). *Dokl. Akad. Nauk SSSR*, **204**, 342–345.
KUSKOV, V. I., KURKUTOVA, E. N., TREUSHNIKOV, E. N., IONOV, V. M., ILYUKIN, V. V. & BELOV, N. V. (1977). *Dokl. Akad. Nauk SSSR*, **234**, 1070–1073.
KUSKOV, V. I., TREUSHNIKOV, E. N., SOBOLEVA, L. V., ILYUKIN, V. V. & BELOV, N. V. (1978*a*). *Dokl. Akad. Nauk SSSR*, **239**, 1097–1100.
KUSKOV, V. I., TREUSHNIKOV, E. N., SOBOLEVA, L. V., ILYUKIN, V. V. & BELOV, N. V. (1978*b*). *Dokl. Akad. Nauk SSSR*, **239**, 594–597.
LEBIODA, Ł. (1972). *Rocz. Chem.* **43**, 373–385.
LEBIODA, Ł. (1977). *Acta Cryst.* B**33**, 1583–1586.
LEBIODA, Ł. & LEWINSKI, K. (1979). To be published.
LEBIODA, Ł. & STADNICKA, K. (1977). *Acta Cryst.* B**33**, 2905–2907.
LEBIODA, Ł., STADNICKA, K. & SLIWINSKI, J. (1979). *Acta Cryst.* B**35**, 157–158.
MCCLELLAN, A. C. (1963). *Tables of Experimental Dipole Moments*. San Francisco: Freeman.
MIKHAILOV, YU. N., IVANOV, S. B., ORLOVA, I. M., PODNIEBIESNIKOVA, G. V. & KUZNIETZOV, V. G. (1976). *Koord. Khim.* **2**, 1570–1573.
MIKHAILOV, YU. N., KUZNIETZOV, V. G. & KOVALEVA, E. S. (1968). *Zh. Strukt. Khim.* **9**, 710–712.
Molecular Structures and Dimensions (1970–1978). Vols. 1–9. Edited by O. KENNARD, F. H. ALLEN, D. G. WATSON & S. WEEDS. Utrecht: Oosthoek.
MOOY, J., KRIEGER, W., HEJEDNJK, D. & STAM, C. H. (1976). *Chem. Phys. Lett.* **29**, 179–183.
PALM, J. H. & MACGILLAVRY, C. H. (1963). *Acta Cryst.* **16**, 963–968.
PANTELEIEV, YU. A. & LIPOVSKIJ, A. A. (1976). *Zh. Strukt. Khim.* **17**, 4–8.
PONOMARENKO, V. I., KURKUTOVA, E. N., PORAI-KOSHITS, M. A., ASLANOV, L. A. & SOULAIMANKULOV, K. (1976). *Dokl. Akad. Nauk SSSR*, **228**, 360–362.
PONOMARENKO, V. I., KURKUTOVA, E. N., PORAI-KOSHITS, M. A. & SOULAIMANKULOV, K. (1977). *Dokl. Akad. Nauk SSSR*, **234**, 1074–1077.
PRYOR, A. W. & SANGER, P. L. (1970). *Acta Cryst.* A**26**, 543–558.
PULLMAN, A. (1974). *Molecular and Quantum Pharmacology*, edited by E. D. BERGMAN & B. PULLMAN, pp. 401–411. Dordrecht: Reidel.
RAU, T. F. & KURKUTOVA, E. N. (1971). *Dokl. Akad. Nauk SSSR*, **200**, 1340–1342.
RODE, B. M. (1976). *Metal Ligand Interactions in Organic Chemistry and Biochemistry*, edited by B. PULLMAN & N. GOLDBLUM, pp. 127–145. Dordrecht: Reidel.
SCHERINGER, C., MULLEN, D., HELLNER, E., HASE, H. L., SCHULTE, K. W. & SCHWEIG, A. (1978). *Acta Cryst.* B**34**, 2241–2243.
TREUSHNIKOV, E. N., KUSKOV, V. I. & BELOV, N. V. (1977). *Kristallografiya*, **22**, 994–1003.
TSINTSADZE, G. V., TSINTSADZE, T. I. & OBERLADZE, F. V. (1974). *Zh. Strukt. Khim.* **15**, 306–307.
VERBIST, J., MEULEMANS, R., PIRET, P. & VAN MEERSSCHE, M. (1970). *Bull. Soc. Chim. Belg.* **79**, 391–395.
VILLIERS, J. P. R. DE & BOEYENS, J. C. A. (1975). *J. Cryst. Mol. Struct.* **5**, 215–226.
YAWNEY, D. B. W. & DOEDENS, R. J. (1970). *Inorg. Chem.* **9**, 1626–1632.

Acta Cryst. (1980). B**36**, 275–287

The Structures of High-Spin (298, 150 K) and Low-Spin (90 K) States and the Spin Phase-Transition Mechanism of a Spin Crossover Complex; Tris(α-picolylamine)iron(II) Chloride–Ethanol

BY MAMI MIKAMI, MICHIKO KONNO AND YOSHIHIKO SAITO

The Institute for Solid State Physics, The University of Tokyo, Roppongi-7, Minato-ku, Tokyo 106, *Japan*

(*Received* 29 *March* 1979; *accepted* 13 *August* 1979)

Abstract

The crystal structures of $[Fe(\alpha\text{-pic})_3]Cl_2.EtOH$, $[Fe(C_6H_8N_2)_3]Cl_2.C_2H_6O$, $[C_{18}H_{24}FeN_6]^{2+}.2Cl^-.C_2H_6O$, in its high-spin state (298, 150 K) and low-spin state (90 K) were determined by X-ray diffraction. The space group is $P2_1/c$, $Z = 4$, over the entire temperature range. At room temperature, $a = 11{\cdot}831\ (3)$, $b = 22{\cdot}021\ (4)$, $c = 11{\cdot}551\ (3)$ Å, $\beta = 124{\cdot}28\ (2)°$, $U = 2485{\cdot}2\ (11)$ Å^3, $D_m = 1{\cdot}33$, $D_c = 1{\cdot}329$ Mg m^{-3} and at

0567-7408/80/020275-13$01.00

90 K, $a = 11{\cdot}616$ (3), $b = 21{\cdot}546$ (3), $c = 11{\cdot}353$ (3) Å, $\beta = 124{\cdot}41$ (2)°, $U = 2344{\cdot}2$ (8) Å^3, $D_c = 1{\cdot}409$ Mg m^{-3}. The structures were solved by the heavy-atom method and refined to $R = 0{\cdot}054$, 0·044 and 0·043 (298, 150 and 90 K, respectively) based on F. Remarkable changes in Fe–N bond lengths were observed. The average Fe–N bond length in the high-spin state (298 K) is 2·195 (5) Å and that in the low-spin state (90 K) is 2·013 (3) Å. The considerable contraction of the Fe–$N_{(pyr)}$ bond, by as much as 0·2 Å, may be ascribed to back bonding as well as to the change in the spin state. All the amino N atoms of the complex are hydrogen bonded to Cl^- forming a two-dimensional network parallel to the (100) plane. Solvate ethanol molecules, hydrogen bonded to Cl^-, exhibit orientational disorder in the high-spin state but a regular arrangement in the low-spin state.

Introduction

Some Fe^{II} and Fe^{III} complexes are known to undergo spin phase transition in certain temperature ranges, alternating between the high-spin state and the low-spin state. Such complexes are called crossover complexes, referring to the crossing of the ground states of the two phases in an energy diagram. The drastic changes in M–L bonds of the spin crossover complexes offer interesting prospects for the study of inorganic chemistry, biochemistry, ligand-field theory and for phase transitions. From the experimental point of view, the crossover complexes can be classified into two groups according to their magnetic properties; the spin-equilibrium type and the spin-transition type. In the former, the magnetic moment varies gradually over a wide temperature range, while the latter type shows marked magnetic susceptibility change in a rather narrow temperature range. The former type appears mostly in Fe^{III} complexes and the latter in Fe^{II} complexes. Many of the spin crossover complexes have been found in pseudo-octahedral Fe^{II} complexes (Goodwin, 1976), which contain bidentate ligands with nitrogen as ligating atoms (diimine). In the low-spin state, all the six $3d$ electrons of Fe^{II} occupy t_{2g} orbitals ($^1A_1$) of O_h parentage, whereas in the high-spin state a different electron configuration, $t_{2g}^4 e_g^2(^5T_2)$ arises. A typical example of an Fe^{II} spin crossover complex is the hemoglobin molecule. In Fe^{II} spin-transition complexes, the magnetic susceptibility changes according to the spin momentum, $S = 0$ to $S = 2$, when a spin phase transition is observed. The physical properties of these complexes have been studied mostly in the last decade (König, 1972; Goodwin, 1976) by means of IR (König & Madeja, 1967*a*,*b*; Sorai & Seki, 1974; Takemoto & Hutchinson, 1973) and Mössbauer spectroscopy and magnetic measurements (König & Madeja, 1967*a*,*b*; König, Madeja & Watson, 1968; König, Ritter & Goodwin, 1976; Renovitch & Baker, 1967; Baker & Bobonich, 1964). Few such crystal structures have been reported so far. For $[Fe(bpy)_2(NCS)_2]$, a preliminary result based on the photographic data was reported by König & Watson (1970). Greenaway & Sinn (1978) recently determined the crystal structures of $[Fe(\alpha\text{-pic})_3]Cl_2.X$ where X = MeOH, $2H_2O$ on the basis of diffractometer data. They found that $[Fe(\alpha\text{-pic})_3]^{2+}$ adopts the *mer* configuration in methanol solvate, whereas it is a *fac* isomer in its dihydrate. The N–H···Cl, N–H···O and O–H···Cl hydrogen bonds are also reported in this series.

These complexes are quite sensitive at the spin crossover to conditions such as counter anions, solvent molecules, hydrogen bonding and ligand substitution or changes in the complex geometry. In order to contribute to the understanding of the nature and mechanism of the spin phase transition, it is necessary to compare the same complex in both its low- and high-spin states at the temperatures below and above the phase transition. Furthermore, it is desirable that neither the environment of the complex nor the symmetry change abruptly between the two states. When such conditions obtain, the changes in the complex may be interpreted directly in terms of the different spin states. Sorai, Ensling & Gütlich (1976) have studied Mössbauer effects for $[Fe(\alpha\text{-pic})_3]Cl_2.EtOH$ and confirmed the coexistence of both high-spin and low-spin phases in the spin-transition temperature range, 100–150 K. This complex is rare in that it undergoes complete spin transition when cooled down to the low-spin state, in contrast to other diimine Fe^{II} spin crossover complexes in which a small percent of the high-spin fraction remains at low temperature (Sorai & Seki, 1974). The dramatic changes in the spin phase transition have been reported on replacement of the central metal atom, solvate molecules and counter anions (Sorai, Ensling & Gütlich, 1976; Sorai, Ensling, Hasselbach & Gütlich, 1977; Gütlich, Link & Steinhäuser, 1978; Renovitch & Baker, 1967). In this paper, we report the crystal structures of $[Fe(\alpha\text{-pic})_3]Cl_2.EtOH$ at 298, 150 and 90 K, determined in order to elucidate the molecular structures and the bonding nature in the two spin states and, further, to clarify the mechanism of the spin phase transition. A preliminary account has been published (Mikami, Konno & Saito, 1979).

Experimental

The complex was synthesized in a nitrogen atmosphere as described by Sorai, Ensling & Gütlich (1976), since $[Fe(\alpha\text{-pic})_3]^{2+}$ is sensitive to oxygen and water. The crystals were grown from a deoxygenated ethanol solution. The rhomboidal crystals are yellow at room temperature and dark red at liquid-nitrogen temperature. The crystal specimens for X-ray work were sealed into Lindemann-glass capillaries in a glove box

filled with dry argon gas. The dimensions of the crystal used for intensity measurements were 0·35 × 0·32 × 0·16 mm. The purity of Fe^{II} was checked by measuring the Mössbauer spectra of a powdered sample taken from the same lot. Direct comparison of the spectra with the previous results of Sorai, Ensling & Gütlich (1976) indicated that the metal complex is in the Fe^{II} high-spin state at room temperature. Also, the transition-temperature range was confirmed by using the magnetic-pendulum method to determine the magnetic moment of representative samples. The results indicated that the temperature should be lower than 95 K in order to obtain significant X-ray diffraction data for the low-spin state.

The cooling device differed in several ways from a commercial device. To provide for smooth gas flow and to avoid growing frost around the sample, the cold N_2 gas was evacuated by a blower at the φ circle. Thus, the cooling of the single crystal was achieved by a cold N_2-gas flow surrounded by a jacket of dry N_2 gas at room temperature, both issuing from an evaporation vessel containing liquid N_2. In this system, the streams of cold and warm N_2 are completely separate. The transfer tube is broadly similar to that described by van Bolhuis (1971). The temperature was fairly stable as the N_2-flow temperature depended mainly on the heating current for evaporation. The temperature was measured by placing a chromel–constantan thermocouple at the orifice of the transfer tube and was controlled by employing a heater inside. The temperature fluctuation in the steady state was ±0·2 K, and the temperature of the specimen was kept in the ranges 90 ± 2 and 150 ± 1 K throughout data collection.

Table 1. *Crystal data*

$[Fe^{II}(C_6H_8N_2)_3]Cl_2.C_2H_6O$, FW 497·2
Monoclinic, space group $P2_1/c$, $Z = 4$

	298 K	150 K	90 K
a (Å)	11·831 (3)	11·537 (4)	11·616 (3)
b (Å)	22·021 (4)	21·825 (6)	21·546 (3)
c (Å)	11·551 (3)	11·420 (4)	11·353 (3)
β (°)	124·28 (2)	123·20 (12)	124·41 (2)
U (Å^3)	2485·2 (11)	2406·2 (12)	2344·2 (8)
D_c (Mg m^{-3})	1·329	1·372	1·409
D_m (Mg m^{-3})	1·33		
μ(Mo $K\alpha$) (mm^{-1})	0·86	0·89	0·91
Scan method	ω–2θ	ω	ω
Scan rate	(4° min^{-1} in $2\theta < 50°$, 2° min^{-1} in $2\theta > 50°$)		
Background counting time (s)	10	15	10
$2\theta_{max}$ (°)	60	55	50
Independent reflections ($\|F\| > 3\sigma$)	3031	4404	3310
Number of parameters	355	355	384
R*	0·054	0·044	0·043
R_2*	0·063	0·046	0·048

* $R = \sum||F_o| - |F_c||/\sum|F_o|$. $R_2 = [\sum(|F_o| - |F_c|)^2/\sum|F_o|^2]^{1/2}$.

The space group and the approximate cell dimensions were determined by oscillation and Weissenberg photographs taken with Cu $K\alpha$ radiation (λ = 1·542 Å). The space group is $P2_1/c$ (systematic absences $0k0$, $k = 2n + 1$; $h0l$, $l = 2n + 1$) and does not change on cooling to the low-spin state. The cell dimensions were later refined by the least-squares method on the basis of eighteen 2θ values measured on the diffractometer. Some of the experimental conditions and the crystal data of the two phases are compared in Table 1.

Intensities at three temperatures were measured on a four-circle diffractometer with graphite-monochromated Mo $K\alpha$ radiation (λ = 0·7107 Å). For data collection at low temperature, two crystals with approximately the same volume were employed. All the reflection peaks were chart-recorded in order to check the pertinent settings and the background balance. The background intensity curve was drawn against sin θ/λ from the plot of counted numbers for zero F value. For some reflections with unequal backgrounds on the two sides of the peaks, the background was estimated from the curve. The standard deviations for the background-corrected intensities were calculated from $\sigma(I) = [I_p + (T_p/2T_b)^2(B_1 + B_2)]$, where I_p is the integrated peak count obtained in scan time T_p; B_1 and B_2 are background counts obtained in scan time T_b. The intensity data were corrected for Lorentz and polarization effects but not for absorption or extinction. Of all the measured intensities, the reflections with $|F| > 3\sigma(|F|)$ were regarded as observed.

Structure determination

High-spin state (298, 150 K)

The structure was solved by conventional heavy-atom methods. The positions of Fe and Cl were deduced from three-dimensional sharpened Patterson maps. The first electron-density maps synthesized using phases based on the heavy atoms revealed all the N and C atoms of the complex. After several cycles of refinement, all the H atoms of the complex could be located from difference syntheses. With R = 0·076, it turned out that the ethanol molecule exhibits orientational disorder. The structure was refined by the full-matrix least-squares program *RADIEL* (Yang, Becker & Coppens, 1979) with equal weight for all the reflections. The populations of disordered ethanol molecules were also refined. Anisotropic thermal parameters were used for all atoms except H and disordered C and O atoms. The final positional parameters are listed in Table 2.* In

* Lists of structure factors, anisotropic thermal parameters at 298 and 90 K, and fractional coordinates and thermal parameters at 150 K have been deposited with the British Library Lending Division as Supplementary Publication No. SUP 34780 (81 pp.). Copies may be obtained through The Executive Secretary, International Union of Crystallography, 5 Abbey Square, Chester CH1 2HU, England.

Table 2. *Fractional atomic coordinates for non-hydrogen* ($\times 10^4$; *for* Fe $\times 10^5$) *and hydrogen atoms* ($\times 10^3$) *in the high-spin state* (298 K)

The populations for disordered atoms are O(*a*) = C*T*(2*a*) = 0·43 (5), O(*b*) = C*T*(2*b*) = 0·28 (2) and O(*c*) = C*T*(2*c*) = 0·29 (4).

	x	*y*	*z*	
Fe^{II}	2724 (8)	13411 (4)	22220 (8)	
Cl(1)	2483 (2)	2731 (1)	1775 (2)	
Cl(2)	−1353 (2)	4313 (1)	3020 (1)	
N(1)	1097 (5)	1375 (2)	949 (5)	
N(2)	2404 (5)	1037 (2)	3656 (5)	
N(3)	859 (5)	2223 (2)	3272 (5)	
N(4)	−1475 (5)	1943 (2)	822 (5)	
N(5)	−691 (5)	484 (2)	1189 (5)	
N(6)	−589 (5)	980 (2)	3364 (5)	
C(1)	2220 (7)	938 (3)	1470 (7)	
C(2)	3056 (6)	921 (3)	3037 (7)	
C(3)	4439 (7)	783 (3)	3815 (9)	
C(4)	5147 (8)	759 (4)	5247 (10)	
C(5)	4489 (9)	881 (4)	5877 (8)	
C(6)	3119 (8)	1015 (3)	5057 (7)	
C(7)	−325 (7)	2590 (3)	2888 (7)	
C(8)	−1522 (7)	2461 (3)	1406 (6)	
C(9)	−2624 (7)	2860 (3)	699 (7)	
C(10)	−3669 (7)	2725 (3)	−632 (8)	
C(11)	−3618 (7)	2202 (3)	−1275 (7)	
C(12)	−2514 (6)	1831 (3)	−508 (6)	
C(13)	−1752 (7)	302 (3)	1382 (7)	
C(14)	−1406 (6)	507 (3)	2782 (6)	
C(15)	−1983 (8)	217 (3)	3428 (7)	
C(16)	−1654 (8)	424 (3)	4707 (8)	
C(17)	−788 (9)	908 (3)	5312 (7)	
C(18)	−261 (7)	1171 (3)	4632 (6)	
O(*a*)	3179 (18)	3896 (9)	3690 (19)	
O(*b*)	4061 (25)	3901 (9)	3565 (25)	
O(*c*)	2988 (38)	3683 (23)	4009 (42)	
C*T*(1)	4528 (17)	3871 (7)	4895 (17)	
C*T*(2*a*)	5074 (35)	3326 (19)	5789 (30)	
C*T*(2*b*)	4339 (46)	3257 (18)	5407 (40)	*U* (Å² ×10³)*
C*T*(2*c*)	5305 (39)	3611 (25)	5960 (37)	
HN(1)	50 (8)	134 (4)	14 (8)	112
HN(2)	142 (6)	171 (3)	100 (6)	49
HN(3)	122 (6)	221 (3)	413 (6)	69
HN(4)	139 (6)	236 (3)	299 (6)	61
HN(5)	−2 (5)	21 (3)	141 (5)	39
HN(6)	−106 (7)	54 (3)	31 (7)	93
H(1)	177 (6)	57 (3)	114 (6)	53
H(2)	286 (7)	106 (3)	116 (7)	82
H(3)	494 (7)	74 (3)	337 (6)	71
H(4)	612 (6)	70 (3)	579 (6)	65
H(5)	483 (6)	88 (3)	671 (6)	58
H(6)	264 (5)	114 (2)	540 (5)	46
H(7)	−74 (7)	248 (3)	345 (7)	89
H(8)	−5 (6)	302 (3)	297 (6)	64
H(9)	−251 (6)	322 (3)	128 (6)	61
H(10)	−461 (8)	296 (3)	−122 (7)	98
H(11)	−421 (6)	206 (3)	−213 (6)	62
H(12)	−237 (6)	146 (2)	−83 (6)	50
H(13)	−271 (7)	53 (3)	62 (7)	90
H(14)	−183 (4)	−9 (2)	129 (4)	15
H(15)	−267 (6)	−11 (2)	295 (6)	49
H(16)	−204 (6)	21 (3)	513 (6)	65
H(17)	−33 (8)	109 (3)	629 (7)	97
H(18)	38 (6)	150 (3)	501 (6)	56

* Isotropic temperature factor.

the last cycle of the refinement, all the parameter shifts were less than one sixth of the corresponding standard deviations. The structure analysis at 150 K was carried out in the same way. *R* converged to 0·054 for the data at 298 K and 0·044 for the data at 150 K.

Low-spin state (90 K)

The structure of the low-spin state was straightforwardly solved by application of the heavy-atom method, since the structure was closely related to that of the high-spin state. The ethanol molecule was regularly arranged and all the H atoms could be located on the difference maps. The refinement was carried out in exactly the same way as that of the high-spin state. The final atomic parameters are tabulated in Table 3.* *R* was reduced to 0·043 (see Table 1). At the final stage of the refinement, the positional shifts were all less than one eighth of the corresponding standard deviations. Atomic scattering factors for Fe^{2+}, Cl^-, N, C_{val} and O and the anomalous-scattering factors for Fe, Cl, N, C and O atoms were taken from *International Tables for X-ray Crystallography* (1974). For hydrogen atoms, scattering factors given by Stewart, Davidson & Simpson (1965) were used.

Description of the structure

The structures comprise octahedral complex cations, chloride anions and ethanol molecules. The arrangement of these structural units is much the same in the low- and high-spin states. Remarkable differences are, however, observed in the geometries of the complex cations, especially in the Fe–N distances. Moreover, the ethanol molecules are arranged regularly in the low-spin state, whereas they exhibit orientational disorder in the high-spin state.

Low-spin state (90 K)

Fig. 1 shows a perspective drawing of the complex cation, together with the numbering scheme. The 2-aminomethylpyridine (α-picolylamine) molecule acts as a bidentate ligand. The three ligand molecules coordinate to the central Fe atom with six N atoms forming a pseudo-octahedral complex ion. This is the *mer* isomer and the complex ion does not have any symmetry. Such a *mer* configuration probably leads to better packing in the crystal lattice than the *fac* configuration in this structure.

The interatomic distances and bond angles within the complex ion are listed in Tables 4 and 5, together with those in the high-spin states (298, 150 K). The

* See deposition footnote.

Table 3. *Fractional atomic coordinates for non-hydrogen* ($\times 10^4$; *for* Fe $\times 10^5$) *and hydrogen atoms* ($\times 10^3$) *in the low-spin state* (90 K)

	x	*y*	*z*	U (Å^2 $\times 10^3$)*
Fe^{II}	2507 (5)	13329 (2)	22300 (5)	
Cl(1)	2681 (1)	2743 (1)	1865 (1)	
Cl(2)	−1374 (1)	4296 (1)	2972 (2)	
N(1)	903 (3)	1472 (1)	935 (3)	
N(2)	2177 (3)	994 (1)	3507 (3)	
N(3)	972 (3)	2158 (1)	3260 (3)	
N(4)	−1446 (3)	1847 (1)	941 (3)	
N(5)	−577 (3)	519 (1)	1213 (3)	
N(6)	−471 (3)	1028 (1)	3376 (3)	
C(1)	2016 (4)	1016 (2)	1307 (4)	
C(2)	2894 (4)	933 (2)	2885 (4)	
C(3)	4299 (4)	806 (2)	3664 (4)	
C(4)	5045 (4)	751 (2)	5133 (5)	
C(5)	4319 (4)	815 (2)	5776 (4)	
C(6)	2903 (4)	938 (2)	4937 (4)	
C(7)	−221 (4)	2550 (2)	2954 (4)	
C(8)	−1462 (4)	2410 (2)	1476 (4)	
C(9)	−2553 (4)	2828 (2)	706 (4)	
C(10)	−3661 (4)	2678 (2)	−670 (4)	
C(11)	−3618 (4)	2117 (2)	−1247 (4)	
C(12)	−2511 (4)	1721 (2)	−418 (4)	
C(13)	−1710 (4)	326 (2)	1363 (4)	
C(14)	−1364 (4)	538 (2)	2789 (4)	
C(15)	−1931 (4)	260 (2)	3453 (4)	
C(16)	−1581 (4)	478 (2)	4765 (4)	
C(17)	−653 (4)	970 (2)	5372 (4)	
C(18)	−131 (4)	1229 (2)	4655 (4)	
O	3057 (4)	3961 (2)	3728 (4)	
C*T*(1)	4481 (5)	3961 (2)	4808 (5)	
C*T*(2)	5065 (5)	3424 (3)	5822 (5)	
HN(1)	17 (4)	146 (2)	5 (4)	20
HN(2)	122 (4)	185 (2)	94 (4)	8
HN(3)	165 (4)	214 (2)	428 (4)	14
HN(4)	149 (4)	235 (2)	300 (4)	16
HN(5)	6 (4)	20 (2)	153 (4)	21
HN(6)	−93 (4)	52 (2)	24 (4)	17
H(1)	154 (4)	66 (2)	88 (4)	13
H(2)	254 (4)	118 (2)	89 (4)	18
H(3)	476 (4)	79 (2)	317 (4)	18
H(4)	607 (5)	68 (2)	577 (5)	27
H(5)	480 (5)	75 (2)	683 (5)	28
H(6)	241 (4)	98 (2)	535 (4)	13
H(7)	−41 (4)	247 (2)	374 (4)	6
H(8)	7 (5)	301 (2)	312 (5)	26
H(9)	−251 (5)	320 (2)	116 (5)	28
H(10)	−451 (5)	298 (2)	−121 (5)	26
H(11)	−440 (4)	201 (2)	−224 (4)	14
H(12)	−244 (4)	134 (2)	−81 (4)	1
H(13)	−263 (4)	51 (2)	57 (4)	4
H(14)	−190 (4)	−11 (2)	126 (4)	4
H(15)	−267 (5)	−10 (2)	292 (5)	28
H(16)	−190 (4)	25 (2)	532 (4)	13
H(17)	−34 (5)	113 (2)	631 (5)	24
H(18)	62 (4)	157 (2)	518 (4)	14
HO	288 (7)	349 (3)	322 (7)	86
H*T*(1)	465 (6)	433 (3)	534 (6)	52
H*T*(2)	493 (5)	402 (2)	419 (5)	40
H*T*(3)	602 (5)	349 (2)	659 (5)	35
H*T*(4)	463 (6)	335 (3)	635 (6)	62
H*T*(5)	498 (6)	300 (3)	534 (6)	60

* Isotropic temperature factor.

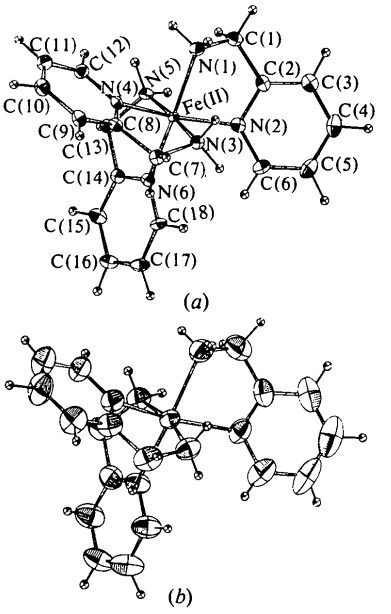

Fig. 1. *ORTEP* drawing of the $[Fe(\alpha\text{-pic})_3]^{2+}$ ion with thermal ellipsoids at 50% probability. (*a*) Low-spin-state complex together with numbering scheme. (*b*) High-spin-state complex.

geometries of the three ligand molecules are nearly the same. The average $Fe-N_{(pyr)}$ distance is 2·002 (4) Å, which is significantly shorter than the average $Fe-N_{(amine)}$ distance of 2·024 (4) Å. The N–Fe–N angle in the chelate ring is 81·6 (2)° on average. The 2-methylpyridine moiety is planar and is tilted with respect to the coordination plane, the average dihedral angle N–C–C–N being about 20°.

Figs. 2 and 3 show projections of the structures along the *b* and *a* axes. Pertinent interatomic distances outside the complex ions are tabulated in Table 9. The complex ions and the chloride ions are held together by Cl···H–N hydrogen bonds to form a layer parallel to the (100) plane. The layers are linked by van der Waals interactions to make up the whole structure. The hydrogen bonds are indicated by broken lines in Figs. 2 and 3. Cl(1) is bonded to N(1) with a N···Cl distance of 3·226 (3) Å. Cl(1) also forms weak hydrogen bonds with the two N(3) atoms of the adjacent complex ions related by a glide plane *c*. Thus, there exist zigzag chains of hydrogen bonds along **c**. The ethanol molecule is bonded to Cl(1) with a Cl···H–O distance of 3·158 (4) Å. Cl(2) is linked to N(1) and N(5) by N–H···Cl hydrogen bonding in the *b* direction. On both sides of the layer formed by the complex cations and chloride ions, the planar pyridine moieties stick out providing hollows surrounded by the chelate rings. The ethanol molecule is accommodated in a hollow and tightly bonded to Cl(1) as described above. All the H atoms of the ethanol molecule were clearly observed. The ethanol molecule adopts the *gauche* conformation with a C–C–O–H torsional angle of 126 (4)°.

Table 4. *Bond distances* (Å) *with e.s.d.'s in parentheses*

	298 K	150 K	90 K
Fe–N(1)	2·176 (7)	2·170 (4)	2·021 (5)
Fe–N(3)	2·184 (5)	2·161 (3)	2·031 (3)
Fe–N(5)	2·180 (5)	2·158 (2)	2·019 (3)
Fe–N(2)	2·200 (5)	2·182 (3)	1·994 (3)
Fe–N(4)	2·208 (5)	2·186 (3)	1·998 (3)
Fe–N(6)	2·220 (7)	2·192 (4)	2·014 (5)
N(1)–N(2)	2·695 (7)	2·709 (4)	2·626 (5)
N(3)–N(4)	2·683 (6)	2·683 (3)	2·629 (4)
N(5)–N(6)	2·679 (9)	2·674 (4)	2·627 (6)
N(1)–N(3)	3·407 (9)	3·387 (5)	2·987 (6)
N(1)–N(4)	3·215 (9)	3·171 (5)	2·850 (6)
N(2)–N(5)	3·353 (6)	3·308 (3)	2·941 (4)
N(2)–N(6)	3·365 (10)	3·315 (5)	2·995 (6)
N(2)–N(3)	3·072 (8)	3·046 (4)	2·809 (5)
N(1)–N(5)	3·010 (9)	2·974 (5)	2·808 (5)
N(4)–N(6)	3·279 (7)	3·249 (4)	2·915 (5)
N(4)–N(5)	3·305 (7)	3·259 (4)	2·991 (4)
N(3)–N(6)	3·262 (8)	3·215 (4)	3·001 (5)
Ligand I			
N(1)–C(1)	1·467 (10)	1·467 (5)	1·483 (6)
N(2)–C(2)	1·339 (12)	1·344 (6)	1·369 (8)
C(1)–C(2)	1·496 (10)	1·508 (4)	1·489 (6)
C(2)–C(3)	1·385 (10)	1·382 (5)	1·375 (6)
C(3)–C(4)	1·371 (13)	1·386 (6)	1·384 (7)
C(4)–C(5)	1·359 (17)	1·371 (8)	1·399 (9)
C(5)–C(6)	1·371 (11)	1·383 (5)	1·383 (6)
C(6)–N(2)	1·339 (8)	1·344 (4)	1·347 (5)
Ligand II			
N(3)–C(7)	1·454 (10)	1·471 (5)	1·486 (6)
N(4)–C(8)	1·341 (9)	1·343 (4)	1·360 (5)
C(7)–C(8)	1·510 (8)	1·511 (4)	1·500 (4)
C(8)–C(9)	1·392 (9)	1·385 (4)	1·389 (5)
C(9)–C(10)	1·355 (9)	1·388 (4)	1·388 (5)
C(10)–C(11)	1·390 (12)	1·385 (5)	1·390 (6)
C(11)–C(12)	1·361 (9)	1·375 (4)	1·378 (5)
C(12)–N(4)	1·342 (7)	1·354 (4)	1·351 (4)
Ligand III			
N(5)–C(13)	1·449 (12)	1·461 (6)	1·479 (7)
N(6)–C(14)	1·318 (8)	1·341 (4)	1·361 (5)
C(13)–C(14)	1·496 (11)	1·515 (5)	1·501 (7)
C(14)–C(15)	1·417 (14)	1·383 (6)	1·387 (8)
C(15)–C(16)	1·376 (13)	1·388 (6)	1·386 (7)
C(16)–C(17)	1·366 (11)	1·384 (5)	1·385 (6)
C(17)–C(18)	1·376 (15)	1·377 (7)	1·378 (8)
C(18)–N(6)	1·354 (10)	1·358 (5)	1·344 (6)

Table 5. *Bond angles* (°) *with e.s.d.'s*

	298 K	150 K	90 K
N(1)–Fe–N(2)	76·0 (2)	77·0 (1)	81·7 (2)
N(3)–Fe–N(4)	75·3 (2)	76·2 (1)	81·5 (1)
N(5)–Fe–N(6)	75·0 (2)	75·9 (1)	81·3 (2)
Ligand I			
Fe–N(1)–C(1)	110·4 (5)	109·0 (2)	108·6 (3)
Fe–N(2)–C(2)	114·7 (5)	114·5 (2)	114·8 (3)
N(1)–C(1)–C(2)	110·0 (7)	110·2 (3)	108·5 (4)
C(1)–C(2)–N(2)	117·0 (6)	116·1 (3)	114·0 (4)
N(2)–C(2)–C(3)	121·4 (7)	122·0 (3)	122·3 (4)
C(2)–C(3)–C(4)	119·1 (10)	119·5 (4)	120·0 (5)
C(3)–C(4)–C(5)	119·6 (9)	118·4 (4)	118·0 (4)
C(4)–C(5)–C(6)	118·9 (8)	119·5 (4)	119·5 (5)
C(5)–C(6)–N(2)	122·5 (9)	122·3 (4)	122·6 (5)
C(6)–N(2)–C(2)	118·5 (6)	118·3 (3)	117·6 (4)
Ligand II			
Fe–N(3)–C(7)	112·0 (4)	111·2 (2)	109·7 (2)
Fe–N(4)–C(8)	115·4 (4)	115·5 (2)	115·1 (2)
N(3)–C(7)–C(8)	111·5 (6)	111·1 (3)	109·0 (3)
C(7)–C(8)–N(4)	116·9 (5)	116·5 (3)	115·6 (3)
N(4)–C(8)–C(9)	122·1 (5)	122·4 (3)	122·3 (3)
C(8)–C(9)–C(10)	118·7 (7)	118·6 (3)	119·6 (4)
C(9)–C(10)–C(11)	120·1 (7)	119·4 (3)	118·4 (4)
C(10)–C(11)–C(12)	117·6 (6)	118·5 (3)	119·0 (3)
C(11)–C(12)–N(4)	124·0 (6)	122·8 (3)	123·7 (4)
C(12)–N(4)–C(8)	117·4 (6)	118·2 (3)	117·0 (3)
Ligand III			
Fe–N(5)–C(13)	112·7 (5)	112·1 (2)	110·2 (3)
Fe–N(6)–C(14)	115·5 (5)	116·2 (2)	114·6 (3)
N(5)–C(13)–C(14)	110·5 (6)	110·5 (3)	109·0 (3)
C(13)–C(14)–N(6)	117·7 (7)	115·6 (3)	115·4 (4)
N(6)–C(14)–C(15)	121·4 (7)	122·7 (3)	122·3 (4)
C(14)–C(15)–C(16)	119·2 (7)	119·4 (3)	119·8 (4)
C(15)–C(16)–C(17)	119·0 (9)	118·4 (4)	117·9 (5)
C(16)–C(17)–C(18)	119·2 (8)	119·2 (4)	119·6 (4)
C(17)–C(18)–N(6)	122·7 (7)	122·9 (3)	123·4 (4)
C(18)–N(6)–C(14)	118·6 (7)	117·5 (3)	117·1 (4)

High-spin state (298, 150 K)

Fig. 2 shows a projection of the structure along **b**. As shown in Table 1, the cell volume expands by about 6%. The bond lengths and angles within the complex ions are listed in Tables 4 and 5. The crystal structures at 298 and 150 K are essentially the same, although some changes in Fe–N and other bond lengths, angles, hydrogen-bond distances and population of disordered ethanol are observed. The changes in the geometry of the complex ion will be discussed in the next section. The general packing features are similar to those in the low-spin state. The ethanol molecules exhibit orientational disorder. The observed electron density can be

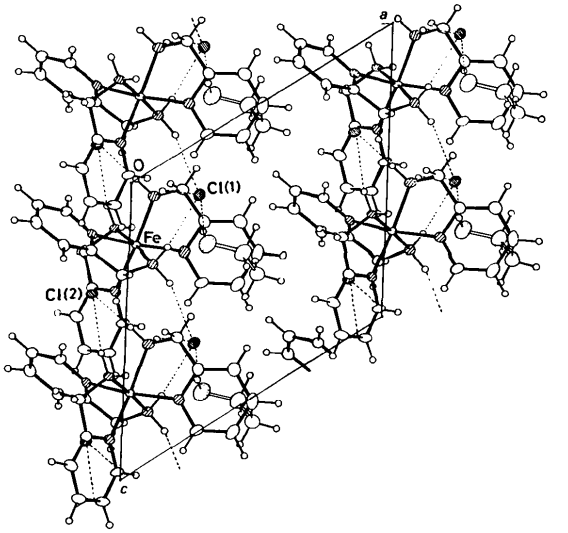

Fig. 2. A projection of the structure along **b** in the low-spin state. Hydrogen bonds are indicated by broken lines.

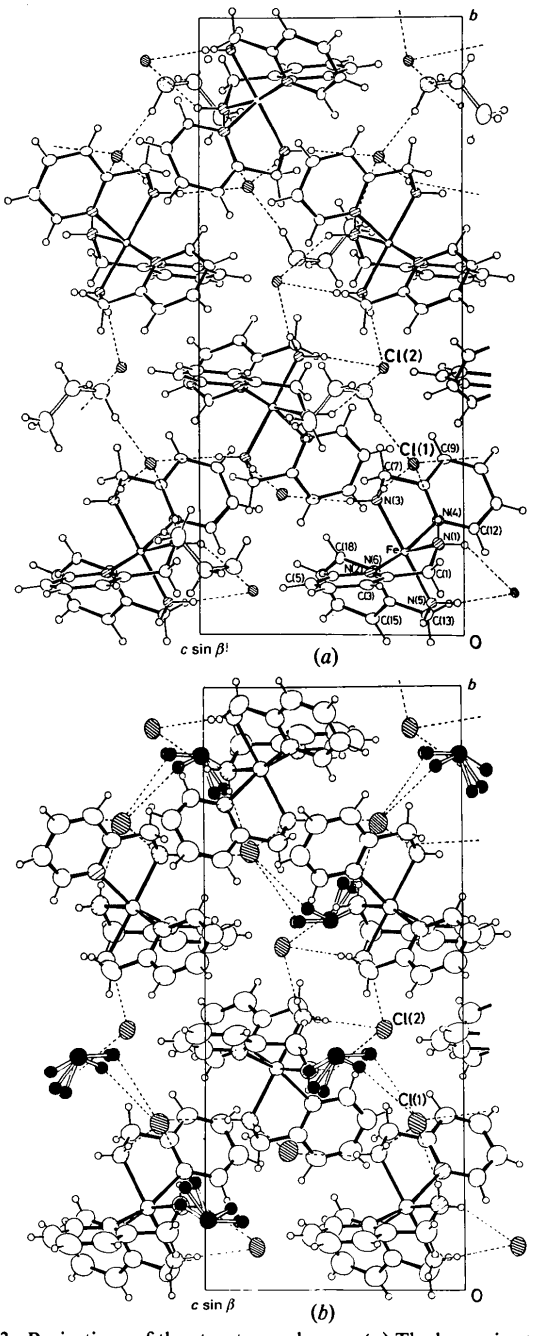

Fig. 3. Projections of the structures along **a**. (*a*) The low-spin state. (*b*) The high-spin state. The disordered ethanol molecules are illustrated as filled circles.

most conveniently accounted for if the ethanol molecule with a *gauche* conformation takes three alternative orientations around the α-carbon atom with different populations. The site with the highest population of 0·43 at 298 K and 0·80 at 150 K is exactly the same as that in the low-spin state. It is to be noted here that the ethanol molecule is always directed towards Cl(1) in all of the three possible orientations.

Results and discussion

Structural changes with the transition

1. Fe–N *bond length.* The Fe–N bond lengths show remarkable changes according to the electron configuration of the two spin states. The average bond lengths are 2·013 (3) and 2·195 (5) Å in the low- and high-spin states, respectively. In the low-spin state Fe–N bonds are shorter by about 0·2 Å compared to those in the high-spin state. This change in the metal–ligand distance is unusually large compared to the temperature dependence of the bond distances observed for transition-metal complexes. For example, in the low-spin complex $[Co(NH_3)_6][Cr(CN)_6]$, the differences in the bond lengths Co–N and Cr–C at 298 and 80 K are 0·010 and 0·009 Å, respectively (Iwata, 1977). Also, the changes in the Fe^{3+} spin crossover complexes, where the difference is found to be 0·05–0·06 Å (Leipoldt & Coppens, 1973; Albertsson & Oskarsson, 1977), are still smaller than those reported here.

Generally, the transition of $3d$ electrons from the e_g orbitals to the t_{2g} orbitals is said to increase the contraction of the ionic radii of the metal. Shannon & Prewitt (1969) have derived the averaged Fe^{2+} radii from several crystal data for octahedral high-spin and low-spin states as 0·91 and 0·75 Å, respectively. The difference of 0·16 Å agrees quite well with the present study. A similar difference has been reported for $[Fe(bpy)_2(NCS)_2]$ (König & Watson, 1970) with average bond lengths of 2·14 (3) and 2·02 (3) Å for the high- and low-spin states from structural analyses based on photographic data. As far as we know, our results are the first direct observations of accurate Fe–N distances of the two spin states within the same complex.

The $Fe-N_{(amine)}$ distance differs significantly from the $Fe-N_{(pyr)}$ distance. The Fe–N distances of the *mer* complex can be classified into three types of bonds according to which of the two N atoms comes in the *trans* position; $Fe-N_{(pyr)}$ may be *trans* to either an $Fe-N_{(pyr)}$ or an $Fe-N_{(amine)}$ and similarly for $Fe-N_{(amine)}$. Table 6 compares the temperature and configurational dependence of Fe–N distances in the present complex and that of *fac*-$[Fe(\alpha\text{-pic})_3]Cl_2.2H_2O$ (Greenaway & Sinn, 1978; Mikami, Konno & Saito, 1979), the latter being in the low-spin state throughout the temperature range. The bond nature in the different spin state or configuration is reflected in the Fe–N distances which show some distinct tendencies: (1) In the high-spin state, $Fe-N_{(pyr)}$ are longer than $Fe-N_{(amine)}$; however, in the low-spin state $Fe-N_{(pyr)}$ are shorter than $Fe-N_{(amine)}$. The considerable shortening of $Fe-N_{(pyr)}$ may be due to the increased back bonding in the low-spin state; *i.e.* electron transfer from the central Fe^{2+} to the π antibonding orbitals of the ligands. The increase in multiple-bond character of the $Fe-N_{(pyr)}$ bond in the low-spin state is further

Table 6. *Average bond lengths of the complex with different spin states and configurations*

	High spin			Low spin
	298 K	*Δr*	150 K	90 K
mer-[Fe(α-pic)$_3$]Cl$_2$.EtOH				
(*A*) $N_{(pyr)}$*trans* $N_{(pyr)}$				
Fe–N(2)	2·200 (5)		2·182 (3)	1·994 (3)
Fe–N(4)	2·208 (5)		2·186 (3)	1·998 (3)
av.	2·204 (5)	0·020	2·184 (3)	1·996 (3)
(*B*) $N_{(am)}$*trans* $N_{(am)}$				
Fe–N(3)	2·184 (5)		2·161 (3)	2·031 (3)
Fe–N(5)	2·180 (5)		2·158 (2)	2·019 (3)
av.	2·182 (5)	0·023	2·159 (3)	2·025 (3)
(*C*) $N_{(am)}$*trans* $N_{(pyr)}$				
$Fe–N(1)_{am}$	2·176 (4)	0·006	2·170 (4)	2·021 (5)
$Fe–N(6)_{pyr}$	2·220 (7)	0·028	2·192 (4)	2·014 (5)
fac-[Fe(α-pic)$_3$]Cl$_2$.2H$_2$O		Low spin		
av. $Fe–N_{(amine)}$	2·027 (2)	0·003	2·024 (4)	
av. $Fe–N_{(pyr)}$	1·985 (2)	0·009	1·976 (4)	

Table 7. *Comparison of metal–ligand bond lengths and angles for various complexes*

		M–L (Å)	*L–M–L* (°)	*L···L* (Å)	Reference
[Co(en)(α-pic)$_2$]$^{3+}$		1·951	83·8	2·606	(1)
[Fe(α-pic)$_3$]Cl$_2$.2H$_2$O		2·006	82·0	2·632	(2)
[Fe(α-pic)$_3$]Cl$_2$.EtOH	90 K	2·013	81·5	2·627	(3)
	150 K	2·175	76·4	2·689	
	298 K	2·195	75·4	2·686	
[Zn(α-pic)$_3$]Cl$_2$.EtOH		2·179	76·4	2·695	(4)
[Fe(α-pic)$_3$]Cl$_2$.MeOH		2·198	75·9	2·703	(2)
[Fe^{III}(S$_2$CNEt$_2$)$_3$]	79 K	2·306	75·9	2·836	(5)
	297 K	2·357	74·3	2·846	
{Fe^{III}[S$_2$CN(CH$_3$)$_2$]$_3$}	150 K	2·339	74·9	2·843	(6)
	295 K	2·395	73·6	2·872	(6)

(1) Sekizaki, 1978; (2) Greenaway & Sinn, 1978; (3) present work; (4) Mikami, Konno & Saito, 1979; (5) Leipoldt & Coppens, 1973; (6) Albertsson & Oskarsson, 1977.

supported by the better planarity of the chelate-ring system. In the case of [Fe(phen)$_2$(NCS)$_2$], partial double-bonding character of $Fe–N_{(phen)}$ in the low-spin state has been proposed (König & Madeja, 1967*b*). (2) In the *mer* configuration complex, $Fe–N_{(pyr)}$ which has $N_{(amine)}$ in the *trans* position is slightly longer than that with $N_{(pyr)}$ in the *trans* position. This is observed in the high- and low-spin states of the ethanol solvate and also in the high-spin state of the methanol solvate. In the case of *mer*-[Fe(α-pic)$_3$]Cl$_2$.MeOH in its high-spin state, the corresponding average bond lengths are 2·199 (4) and 2·223 (4) Å for $Fe–N_{(pyr)}$ and 2·182 (5) and 2·178 Å for $Fe–N_{(amine)}$ (Greenaway & Sinn, 1978). (3) In the low-spin-state complex, comparing *mer*-[Fe(α-pic)$_3$]Cl$_2$.EtOH and *fac*-[Fe(α-pic)$_3$]Cl$_2$.2H$_2$O, all the Fe–N bond lengths of the *fac* complex are shorter than the corresponding bonds of the *mer* complex. The strength of hydrogen bonds may affect the configuration of the complex. Whether the *mer* isomer or the *fac* isomer is more stable in the low-spin state may be attributed to the relative stabilized energy of both kinematical and thermodynamical origin. (4) The difference in the bond distances of Fe–N at 298 and 150 K are shown as *Δr* in Table 6. The *Δr* values of the (*C*) group of the high-spin state *mer*-[Fe(α-pic)$_3$]Cl$_2$.EtOH are 0·006 Å for $Fe–N_{(amine)}$ and 0·028 Å for $Fe–N_{(pyr)}$ bonds. On the other hand, in the low-spin state *fac*-[Fe(α-pic)$_3$]Cl$_2$.2H$_2$O, *Δr* for $Fe–N_{(amine)}$ is 0·003 Å and that for $Fe–N_{(pyr)}$ is 0·009 Å. The amount of temperature-dependent difference, *Δr*, in the two complexes again appears to be due to different electron configurations. The longer Fe–N bonds, accompanied by a smaller force constant in the high-spin state, may be more affected by thermal vibration.

2. *Chelate-ring system.* The N–Fe–N bite angle decreases by about 6° and the Fe–N distance increases by 0·2 Å on going from the low- to the high-spin state, while the mean N···N distance in the chelate ring does not change very much, as seen from Tables 4 and 5. A similar trend for the *M–L* bond lengths and *L–M–L* angle is observed in analogous complexes and in the Fe^{III} spin crossover complexes as shown in Table 7.

Another significant change is observed in the elongation of the $N_{(pyr)}$–C bond in the low-spin state by 0·030 Å, which reflects the conjugation with the $Fe–N_{(pyr)}$ bond. The average $N_{(pyr)}$–C bond lengths in the five-membered rings are 1·333 (10), 1·343 (5) and 1·363 (6) Å at 298, 150 and 90 K, respectively. The values fall between single- and double-bond distances. On the other hand, the corresponding mean $N_{(amine)}$–C bond lengths are 1·457 (11), 1·466 (5) and 1·483 (6) Å, becoming longer with lower temperature. In the low-spin state, the contraction of the Fe–N bond arising from the increase in d–π interaction, as well as σ donation, results in the decrease of bond order in adjacent N–C bonds in the five-membered chelate ring.

The 2-methylpyridine moiety shows good planarity. The best plane and atomic shifts are shown in Table 8. In the chelate rings II and III, the Fe atom deviates by 0·14 Å from the best plane of the 2-methylpyridine moiety in the high-spin state, whereas the deviation is only 0·05 Å in the low-spin state. The chelate ring I is rather an exception: it is much more distorted, the deviation of Fe being as large as 0·36 Å. The planarity of ligand I seems to be broken by the steric interaction between the two pyridine rings of ligand I related by a center of symmetry. In addition, a relatively strong hydrogen bond of 3·226 (3) Å exists between N(1) and Cl(1). In the case of [Fe(tripyam)$_2$](ClO$_4$), the deviation of the non-hydrogen atoms and Fe^{2+} from the pyridine plane are smaller than 0·01 and 0·05 Å, respectively (Kucharski, McWhinnie & White, 1978).

Table 8. *Deviations of atoms from the least-squares planes through the six atoms of the pyridine rings*

Equations of the least-squares planes are referred to the orthogonal coordinate system defined by $X \| a$, $Y \| b^*$ and $Z \| c^*$. The atoms with asterisks were included in the calculations of the least-squares planes.

	298 K	150 K	90 K
Ligand I			
N(2)*	0·001 (6)	0·010 (7)	0·004 (5)
C(2)*	0·001 (7)	−0·009 (7)	−0·006 (6)
C(3)*	−0·004 (8)	0·002 (7)	0·006 (6)
C(4)*	0·006 (9)	0·005 (8)	−0·004 (6)
C(5)*	−0·004 (9)	−0·005 (8)	0·002 (6)
C(6)*	0·001 (8)	−0·003 (7)	−0·002 (6)
Fe	−0·214 (3)	−0·228 (6)	−0·363 (4)
N(1)	−0·653 (6)	−0·712 (7)	−0·791 (5)
C(1)	0·027 (8)	−0·001 (7)	−0·032 (6)
Ligand II			
N(4)*	−0·018 (12)	−0·009 (13)	−0·018 (15)
C(8)*	0·012 (13)	0·009 (13)	0·015 (15)
C(9)*	0·005 (14)	0·003 (13)	0·002 (15)
C(10)*	−0·008 (14)	−0·021 (13)	−0·020 (15)
C(11)*	0·008 (14)	0·010 (13)	0·012 (15)
C(12)*	−0·002 (13)	0·013 (13)	0·011 (15)
Fe	−0·210 (10)	−0·097 (12)	0·048 (14)
N(3)	0·427 (12)	0·493 (13)	0·607 (15)
C(7)	0·034 (14)	0·019 (13)	0·069 (15)
Ligand III			
N(6)*	−0·013 (10)	0·002 (5)	−0·007 (6)
C(14)*	0·010 (11)	−0·002 (5)	0·006 (7)
C(15)*	−0·002 (12)	0·004 (6)	0·001 (7)
C(16)*	−0·002 (12)	−0·006 (6)	−0·006 (7)
C(17)*	−0·002 (12)	0·006 (6)	0·005 (7)
C(18)*	0·009 (11)	−0·004 (6)	0·001 (7)
Fe	0·099 (8)	0·159 (4)	0·057 (5)
N(5)	0·525 (10)	0·601 (5)	0·549 (6)
C(13)	−0·011 (11)	0·001 (6)	0·003 (7)

Equations of least-squares planes (X, Y and Z are in Å)

Ligand I	$0{\cdot}2344X + 0{\cdot}9710Y + 0{\cdot}0465Z =$	2·4883 (298 K)
	$0{\cdot}2497X + 0{\cdot}9681Y + 0{\cdot}0232Z =$	2·3994 (150 K)
	$0{\cdot}1610X + 0{\cdot}9817Y + 0{\cdot}1015Z =$	2·4849 (90 K)
Ligand II	$-0{\cdot}7982X - 0{\cdot}4982Y + 0{\cdot}3387Z =$	−0·0654 (298 K)
	$-0{\cdot}8183X - 0{\cdot}4645Y + 0{\cdot}3385Z =$	0·1180 (150 K)
	$-0{\cdot}8361X - 0{\cdot}4215Y + 0{\cdot}3512Z =$	0·5239 (90 K)
Ligand III	$-0{\cdot}6302X + 0{\cdot}6235Y - 0{\cdot}4627Z =$	1·6683 (298 K)
	$-0{\cdot}6552X + 0{\cdot}6269Y - 0{\cdot}4216Z =$	1·8008 (150 K)
	$-0{\cdot}6194X + 0{\cdot}6379Y - 0{\cdot}4577Z =$	1·6392 (90 K)

3. *Hydrogen bonding and the ethanol molecule.* All the amino N atoms of the complex are hydrogen bonded to a Cl^- ion in the two spin states. Hydrogen-bond distances at three different temperatures are compared in Table 9. Cl(1) is hydrogen bonded to N(1) with N···Cl distances of 3·226–3·286 Å, and is also bonded to the O atom of ethanol. The linear chain of hydrogen bonds runs along **c**, involving Cl(1) and N(3) alternately in a zigzag way (Fig. 2). These hydrogen bonds are rather long; the distances range from 3·363 to 3·417 Å. On the other hand, Cl(2) and N(5) form two hydrogen bonds in the *b* and *c* directions with distances 3·250–3·314 Å, linking the neighboring complexes related by a symmetry center. Thus, the two-dimensional hydrogen-bond network is formed parallel to the (100) plane.

Close examination of the hydrogen-bond distances at 150 and 90 K, just above and below the spin phase-transition temperature, revealed interesting aspects, as follows. The N—H···Cl hydrogen-bond distances are longer by 0·011–0·026 Å at 90 K than those at 150 K in the *c* direction. The ordering of ethanol would cause a stronger O—H···Cl and a weaker N—H···Cl hydrogen bond through the change of polarization of the Cl^- ion. In the *b* direction, stronger hydrogen bonds tend to increase electron density on amino N atoms resulting in a short Fe—N bond.

In the *a* direction, where no hydrogen-bond network exists, there seem to be some weak interactions between hydrogen-bonded sheets. The pyridine ring of ligand I and that related by a symmetry center in the next sheet have the closest intermolecular contact and, although they do not overlap, the distance between these two pyridine-ring planes is 3·18 Å. This is the distance within which the interaction of overlapping π-electron orbitals is possible.

The O—H···Cl distances are 3·180 (14), 3·164 (4) and 3·158 (4) Å at 298, 150 and 90 K. These are the distances involving the highest population of ethanol sites at each temperature (0·43, 0·8 and 1·0, respectively). It may be noted that the distances become shorter as the population increases, suggesting stronger hydrogen bonding in the ordered state of ethanol. Moreover, the O—H bond length appears to elongate with a stronger O—H···Cl hydrogen bond at 90 K.

Table 9. *Intermolecular distances* (Å) *shorter than* ~3·8 Å

Symmetry code

none	x, y, z	(iii)	$-x, -y, 1-z$
(i)	$x, \frac{1}{2}-y, \frac{1}{2}+z$	(iv)	$1-x, -y, 1-z$
(ii)	$-x, \frac{1}{2}+y, \frac{1}{2}-z$	(v)	$x, \frac{1}{2}-y, -\frac{1}{2}+z$

	298 K	150 K	90 K
Cl(2)···C(12^{i})	3·711 (8)	3·626 (4)	3·553 (5)
C(6)···Cl(1^{i})	3·717 (9)	3·681 (4)	3·685 (5)
C(7)···N(1^{i})	3·718 (8)	3·621 (4)	3·549 (5)
C(16)···Cl(2^{i})	3·684 (11)	3·587 (5)	3·544 (6)
C(17)···Cl(2^{i})	3·581 (11)	3·520 (5)	3·540 (6)
C(17)···C(9^{i})	3·658 (13)	3·568 (6)	3·560 (7)
C(18)···Cl(1^{i})	3·667 (7)	3·635 (3)	3·552 (4)
O(*a*)···C(13^{ii})	3·505 (16)	3·443 (5)	3·400(6)
O(*a*)···C(15^{ii})	3·541 (15)	3·610 (5)	3·551 (5)
C(6)···C(16^{iii})	3·695 (12)	3·683 (6)	3·517 (6)
C(14)···C(16^{iii})	3·726 (9)	3·639 (5)	3·670 (5)
C(3)···C(4^{iv})	3·515 (11)	3·512 (5)	3·538 (6)
C(4)···C(4^{iv})	3·378 (16)	3·282 (7)	3·244 (9)
C(5)···O(*b*^{i})	3·45 (3)	3·37 (6)	
C(6)···O(*b*^{i})	3·55 (3)	3·53 (5)	
O(*c*)···C(1^{i})	3·54 (4)	3·87 (4)	
O(*c*)···C(13^{ii})	3·78 (3)	3·40 (3)	

Table 9 (*cont.*)

Hydrogen-bond distances

	298 K			150 K			90 K		
N–H···Cl	N···Cl	N–H	H···Cl	N···Cl	N–H	H···Cl	N···Cl	N–H	H···Cl
N(1)–HN(2)···Cl(1)	3·279 (6)	0·83 (6)	2·48 (5)	3·286 (3)	0·87 (4)	2·43 (4)	3·226 (3)	0·90 (4)	2·38 (4)
N(3)–HN(4)···Cl(1)	3·417 (8)	0·91 (9)	2·52 (9)	3·378 (4)	0·92 (6)	2·46 (6)	3·404 (5)	0·90 (6)	2·51 (6)
N(3^{v})–HN(3)···Cl(1)	3·363 (5)	0·83 (7)	2·54 (6)	3·376 (3)	0·82 (4)	2·58 (5)	3·399 (4)	0·96 (4)	2·48 (4)
N(1^{i})–HN(1)···Cl(2)	3·329 (5)	0·80 (7)	2·61 (7)	3·305 (3)	0·84 (3)	2·55 (3)	3·316 (3)	0·95 (4)	2·52 (4)
N(5^{i})–HN(6)···Cl(2)	3·314 (6)	0·86 (8)	2·49 (9)	3·271 (3)	0·84 (5)	2·46 (5)	3·272 (4)	0·93 (5)	2·36 (5)
N(5^{ii})–HN(5)···Cl(2)	3·291 (5)	0·91 (6)	2·40 (5)	3·278 (3)	0·90 (3)	2·41 (4)	3·250 (3)	0·92 (4)	2·33 (5)
O–H···Cl	O···Cl			O···Cl	O–H	H···Cl	O···Cl	O–H	H···Cl
O(*a*)–HO···Cl(1)	3·180 (14)			3·164 (4)	0·81 (5)	2·37 (5)	3·158 (4)	1·04 (7)	2·14 (8)

As mentioned earlier, the ethanol molecule is linked to the complex ion by two hydrogen bonds in an O–H···Cl···H–N sequence through the Cl^- ion and exhibits orientational disorder only in the high-spin state. In order to investigate the behavior of the ethanol molecule, the following measurements were carried out. Twelve reflections which were sensitive to the population of the ethanol sites were selected by structure-factor calculations. The intensities of these particular reflections varied by 10–25% in calculations. The temperature dependence of the intensities of these reflections was measured at eight fixed temperatures between 140 and 298 K. As shown in Fig. 4, all the reflections indicated a similar intensity variation to that estimated by calculations. The ethanol molecules,

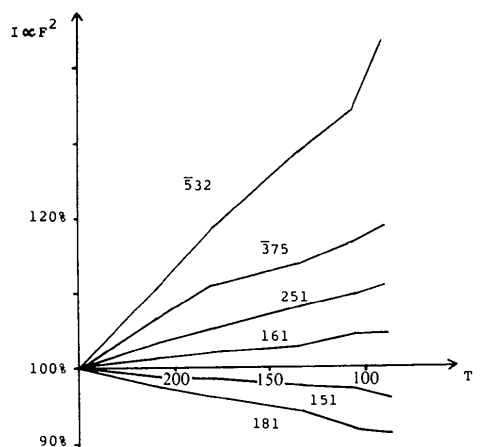

h k l	Fo_{298}	Fc'
$\bar{5}$ 3 2	59.0	64.5
$\bar{3}$ 7 5	100.7	99.0
2 5 1	89.0	95.4
1 6 1	106.4	106.4
1 5 1	88.4	80.1
1 8 1	62.1	57.4

Fig. 4. Temperature dependence of the intensities for reflections sensitive to the disordered ethanol molecule. *Fo*: observed structure factors at 298 K. *Fc'*: calculated structure factors assuming ordered ethanol at 298 K.

which are distributed over three sites at 298 K with an approximate population ratio of 3:2:2, gradually converge to one site with the highest population with lowering of temperature. The structural analysis at 150 K revealed that this population ratio changes to 8:1:1 just above the spin-transition temperature. In the low-spin state, the ethanol molecule occupies, with 100% occupancy, the site that is most populated in the high-spin structure. Thus, the gradual ordering of the ethanol molecule takes place over a wide temperature range.

Thermal motion

The mean coefficients α_{hkl} of thermal expansion per K normal to the plane (*hkl*) were obtained for 11 reflections in the high-spin state. $\alpha_{hkl} = (\sin\theta_1 - \sin\theta_2)/\sin\theta_{1,2}(T_2 - T_1)$ were derived from the gradients of linear plots in the temperature range 298–150 K. These coefficients can be expressed by the components $[\alpha_{ij}]$ of the tensor as follows. For a monoclinic system, $\alpha_{hkl} = \alpha_{11}\cos^2\alpha + \alpha_{22}\cos^2\beta + \alpha_{33}\cos^2\gamma + 2\alpha_{13}\cos\alpha\cos\gamma$, where cos α *etc.* stand for direction cosines between the unit normal to the plane (*hkl*) and the orthogonal coordinate axes (*OX* ∥*a*, *OY* ∥*b** and *OZ* ∥*c**). Principal coefficients of the thermal expansion were derived by the least-squares program *TEC* (Konno & Mikami, 1979) based on these 11 reflections, as shown in Table 10. The principle axis corresponding to the largest expansion is inclined by 12·5° from **a** (see Fig. 5). This indicates that thermal vibration is largest in the *a* direction, along which no hydrogen bonds exist. The expansion figure (Fig. 5) appears to be determined by the overall packing arrangement in the crystal lattice rather than molecular symmetry. A similar anisotropy in the thermal-expansion coefficients is reported for ferrocene with magnitude $\alpha_1 = 15{\cdot}0 \times 10^{-5}$, $\alpha_2 = 3{\cdot}6 \times 10^{-5}$ and $\alpha_3 = 8{\cdot}2 \times 10^{-5}$ K^{-1} (Edwards, Kington & Mason, 1960; Calvarin & Berar, 1975).

The lattice constants at eight different temperatures were obtained based on 16 reflections (Table 11). All the cell constants showed a linear decrease as the

Table 10. *Values of the thermal-expansion coefficients* ($\times 10^5$ K^{-1})

h k l	α_{obs}	α_{calc}	h k l	α_{obs}	α_{calc}
0 14 0	4·8	4·4	$\bar{4}$ 8 10	5·1	4·5
$\bar{6}$ 0 12	6·6	6·7	$\bar{7}$ 9 4	12·6	12·9
9 0 $\bar{6}$	17·2	17·4	7 3 2	3·6	3·6
6 2 5	−0·5	−0·0	$\bar{5}$ 16 4	7·5	8·0
$\bar{6}$ 6 11	7·5	7·5	3 18 4	2·2	2·3
10 5 $\bar{2}$	11·5	10·7			

Components of tensor

$\alpha_{11} = 16{\cdot}5 \pm 0{\cdot}4$ $\quad$ $\alpha_{33} = -1{\cdot}2 \pm 0{\cdot}4$

$\alpha_{22} = 4{\cdot}4 \pm 0{\cdot}4$ $\quad$ $\alpha_{13} = -4{\cdot}1 \pm 0{\cdot}3$

Principal coefficients of the thermal expansion

$\alpha_1 = 17{\cdot}4 \pm 0{\cdot}4$ $\quad$ $\alpha_3 = -2{\cdot}1 \pm 0{\cdot}4$

$\alpha_2 = 4{\cdot}4 \pm 0{\cdot}4$ $\quad$ $\psi = -12°$

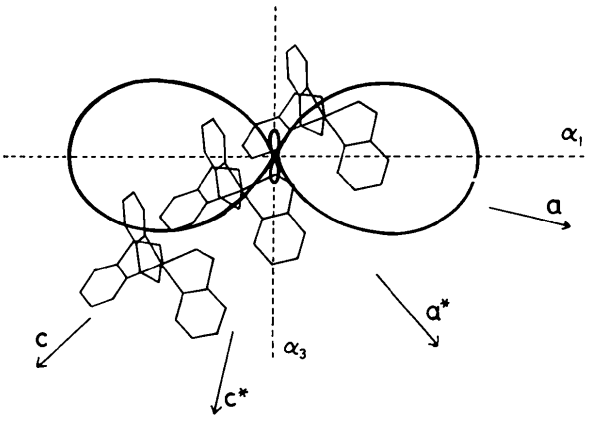

Fig. 5. Anisotropy of the thermal expansion on the (010) plane.

Table 11. *Temperature dependence of the lattice constants*

K	a (Å)	b (Å)	c (Å)	β (°)	U (Å^3)
298	11·831 (3)	22·021 (4)	11·551 (3)	124·28 (2)	2485·2 (11)
250	11·751 (2)	21·964 (3)	11·529 (2)	124·06 (1)	2465·0 (7)
225	11·675 (2)	21·934 (2)	11·493 (2)	123·75 (1)	2447·6 (5)
200	11·640 (2)	21·927 (3)	11·475 (2)	123·60 (1)	2439·5 (6)
180	11·579 (3)	21·903 (4)	11·438 (3)	123·32 (2)	2424·2 (8)
160	11·547 (4)	21·840 (7)	11·425 (4)	123·21 (3)	2410·7 (13)
150	11·537 (5)	21·825 (8)	11·420 (5)	123·20 (4)	2406·2 (16)
90	11·616 (3)	21·546 (3)	11·353 (3)	124·41 (2)	2344·2 (8)

temperature was lowered in the high-spin region. However, in the spin-phase-transition-temperature region, abrupt changes took place: 1·3% shrinkage in the b and, surprisingly, 0·7% elongation in the a axes. The interplanar distance between the hydrogen-bonded sheets parallel to the (100) plane decreases linearly (9·77–9·58 Å) with lowering of temperature. As the complex changes its spin state from high to low, the pyridine ring of ligand I becomes more coplanar with the ac plane. This results in a larger β angle and appears to slide the sheets a little in the c direction. So, without much change in the interplanar distance, the a lattice constant seems to increase on going to the low-spin state. Thus, some rearrangement of the complex and ordered ethanol seems to occur in this region. The cell volume contracts by 6% on changing from the high- to the low-spin state.

The thermal motion of the molecule has been analyzed in terms of the rigid-body tensors **T**, **L** and **S** (Schomaker & Trueblood, 1968). Rigid-body parameters at 298, 150 and 90 K are shown in Table 12. The r.m.s. discrepancies ΔU_{ij} between the observed and calculated thermal parameters are 63 × 10^{-4}, 38 × 10^{-4} and 27 × 10^{-4} Å^2 at 298, 150 and 90 K, respectively. Thus, the molecule is not expected to behave strictly as a rigid body. The correction of the rigid-body tensor gave no significantly systematic changes in molecular geometry. However, apart from the precise consideration of a slight difference in anharmonicity or bond character at various temperatures, the rigid-body approximation seems to apply somewhat better at lower temperatures. The overall translation of the complex molecule was largest in the a direction. The N—H···Cl hydrogen bond may be expected to prevent the molecule from undertaking rigid-body libration. The rigid-body discrepancies, calculated by the condition $\Delta_{AB} = z^2_{AB} - z^2_{BA}$ (Rosenfield, Trueblood & Dunitz, 1978; Hirshfeld, 1976), between other ligands were observed to be large compared to those within a ligand. The largest principal axis of the thermal motion of the C atoms in ligand I is almost parallel to the pyridine ring, although those of the C atoms of ligands II and III are perpendicular to their pyridine rings. The pyridine ring of ligand I and that related by a symmetry center are in closest proximity at 3·24 Å. So the thermal motion perpendicular to the plane is expected to be reduced by the steric repulsion in ligand I. The thermal-motion ellipsoids were plotted by *ORTEP* as shown in Fig. 1 (Johnson, 1965). The root-mean-square amplitudes of the thermal motions of the atoms are reduced at 90 K to 35–50% of that at room temperature.

The spin phase transition

The present X-ray studies revealed the existence of hydrogen bonds between the complexes and the solvate ethanol molecules through Cl^- ions. The structural differences in the two spin states are not only the remarkable changes in the Fe—N bond nature in the complex but also the variation of the disorder of the ethanol molecules. The strong correlation between the Fe^{2+} spin phase transition and the rotational ground state of the solvate molecule (EtOH, MeOH) was proved by a Mössbauer study (Gütlich, 1979). When

the temperature is lowered in the high-spin region, the orientationally disordered ethanol molecules gradually tend to arrange regularly. At temperatures around 150 K, the spin phase transition begins to take place as the dominant site of disordered ethanol has 80% occupancy and the ligand-field strength may increase with a little shortening of the Fe–N bonds. In other words, the ordering of the ethanol molecule seems to act as an initiator or trigger to the Fe^{2+} spin transition. The complex and ethanol interact through hydrogen bonds when the spin phase transition and the order–disorder transition of ethanol take place. In the ethanol solvate, some weak interaction between the hydrogen-bonded sheets may also possibly contribute to the cooperative nature. In the case of the methanol solvate, which has similar hydrogen bonds to that of the ethanol solvate (Katz & Strouse, 1979), the spin phase transition occurs more gradually as a function of temperature (Sorai, Ensling, Hasselbach & Gütlich, 1977). The methanol molecule is expected, from the value of the binding energy, to have a stronger Cl–O–H hydrogen bond than ethanol and, in fact, a shorter hydrogen bond in the methanol solvate was observed. However, the hydrogen bonds in the *c* direction, which seem to play an important role in the cooperative transition, were longer in the methanol solvate compared with those in the ethanol solvate. In the spin-transition temperature region, the coexistence of the high- and low-spin states was confirmed by Mössbauer study. The splitting of X-ray diffraction peaks arising from the high-spin and low-spin fraction was also observed in this region. This seems to support the cooperative nature of this spin transition and, moreover, suggests that the domains made up of like spin would include about five hundred complex cations. The present complex is known to be a rare example that undergoes complete spin transition by temperature variation. This is also true when the complex is diluted with a diamagnetic zinc complex to even less than 0·1% (Gütlich, Link & Steinhäuser, 1978; Sorai, Ensling & Gütlich, 1976). We have also determined the crystal structure of an analogous zinc picoline complex at room temperature (Mikami, Konno & Saito, 1980) and found that it is isostructural with the Fe^{2+} complex in its high-spin state. A similar orientational disorder in ethanol was also observed. The interactions between the complexes and that

Table 12. *Rigid-body thermal parameters*

(*a*) Principal axes of the molecule in the form $La + Mb + Nc$

	Moment of inertia (a.u. Å²)	*L*	*M*	*N*
	1559·3	0·0958	−0·0183	0·0521
90 K	2259·8	−0·0180	−0·0224	0·0652
	2955·9	0·0373	0·0363	0·0666
	1702·6	0·0945	−0·0187	0·0505
150 K	2477·2	−0·0214	−0·0230	0·0617
	3235·7	0·0366	0·0349	0·0678
	1707·7	0·0939	−0·0179	0·0506
298 K	2506·6	−0·0191	−0·0237	0·0611
	3263·3	0·0359	0·0343	0·0686

(*b*) Molecular vibrational tensors

	T × 10⁴ (Å²)			**L** × 10 (deg²)		
	160 (6)	−7 (6)	11 (7)	27 (5)	1 (4)	−7 (3)
90 K		119 (7)	0 (7)		19 (3)	−8 (2)
			106 (8)			21 (2)
	223 (9)	−42 (9)	−13 (9)	31 (7)	8 (6)	−12 (4)
150 K		197 (10)	−20 (10)		24 (4)	−10 (3)
			141 (12)			30 (3)
	439 (15)	−37 (14)	−4 (15)	63 (12)	27 (9)	−23 (7)
298 K		406 (17)	−11 (17)		73 (7)	−22 (5)
			318 (20)			82 (5)

Table 12 (*cont.*)

(*c*) Eigenvalues and direction cosines of **T** and **L**

R.m.s amplitude	Direction cosines			R.m.s. amplitude	Direction cosines		
90 K							
0·102 Å	−0·2080	−0·1007	0·9729	1·03°	−0·2569	−0·6485	−0·7166
0·109	−0·1250	−0·9838	−0·1285	1·50	−0·7032	0·6341	−0·3218
0·128	0·9701	−0·1483	0·1920	1·83	0·6630	0·4212	−0·6188
150 K							
0·112	0·3020	0·4338	0·8489	1·29	0·0417	0·7920	0·6091
0·135	−0·5190	−0·6721	−0·5281	1·39	−0·7782	0·4081	−0·4774
0·160	0·7996	−0·6001	0·0222	2·21	−0·6267	−0·4541	0·6333
298 K							
0·178	0·0763	0·1470	0·9862	2·00	−0·8027	0·5820	−0·1304
0·196	−0·5427	−0·8236	0·1648	2·39	−0·2935	−0·5757	−0·7632
0·215	0·8364	−0·5478	0·0170	3·48	−0·5193	−0·5743	0·6329

R.m.s. deviation between obs. and calc. U_{ij} (Å²)

298 K 63 × 10⁻⁴ 150 K 38 × 10⁻⁴ 90 K 27 × 10⁻⁴

between the complex and the order–disorder variation of the ethanol molecule through hydrogen bonds seem to cause the cooperative nature of this spin phase transition.

References

ALBERTSSON, J. & OSKARSSON, A. (1977). *Acta Cryst.* B**33**, 1871–1877.

BAKER, W. A. JR & BOBONICH, H. M. (1964). *Inorg. Chem.* **3**, 1184–1188.

BOLHUIS, F. VAN (1971). *J. Appl. Cryst.* **4**, 263–264.

CALVARIN, G. & BERAR, J. F. (1975). *J. Appl. Cryst.* **8**, 380–385.

EDWARDS, J. W., KINGTON, G. L. & MASON, R. (1960). *Trans. Faraday Soc.* **56**, 660–667.

GOODWIN, H. A. (1976). *Coord. Chem. Rev.* **18**, 293–325.

GREENAWAY, A. M. & SINN, E. (1978). *J. Am. Chem. Soc.* **100**, 8080–8084.

GÜTLICH, P. (1979). *J. Phys. (Paris) Colloq.* **C2**, 378–385.

GÜTLICH, P., LINK, R. & STEINHÄUSER, H. G. (1978). *Inorg. Chem.* **17**, 2509–2514.

HIRSHFELD, F. L. (1976). *Acta Cryst.* A**32**, 239–244.

International Tables for X-ray Crystallography (1974). Vol. IV. Birmingham: Kynoch Press.

IWATA, M. (1977). *Acta Cryst.* B**33**, 59–69.

JOHNSON, C. K. (1965). *ORTEP.* Report ORNL-3794. Oak Ridge National Laboratory, Tennessee.

KATZ, B. A. & STROUSE, C. E. (1979). *Am. Chem. Soc. Abstr.* (Honolulu).

KÖNIG, E. (1972). *Ber. Bunsenges. Phys. Chem.* **76**, 975–990.

KÖNIG, E. & MADEJA, K. (1967*a*). *Inorg. Chem.* **6**, 48–55.

KÖNIG, E. & MADEJA, K. (1967*b*). *Spectrochim. Acta Part A*, **23**, 45–54.

KÖNIG, E., MADEJA, K. & WATSON, K. J. (1968). *J. Am. Chem. Soc.* **90**, 1146–1153.

KÖNIG, E., RITTER, G. & GOODWIN, H. A. (1976). *Chem. Phys. Lett.* **44**, 100–103.

KÖNIG, E. & WATSON, K. J. (1970). *Chem. Phys. Lett.* **6**, 457–459.

KONNO, M. & MIKAMI, M. (1979). Unpublished.

KUCHARSKI, E. S., MCWHINNIE, W. R. & WHITE, A. H. (1978). *Aust. J. Chem.* **31**, 53–56.

LEIPOLDT, J. G. & COPPENS, P. (1973). *Inorg. Chem.* **12**, 2269–2274.

MIKAMI, M., KONNO, M. & SAITO, Y. (1979). *Chem. Phys. Lett.* **63**, 566–569.

MIKAMI, M., KONNO, M. & SAITO, Y. (1980). To be published.

RENOVITCH, G. A. & BAKER, W. A. JR (1967). *J. Am. Chem. Soc.* **89**, 6377–6378.

ROSENFIELD, R. E. JR, TRUEBLOOD, K. N. & DUNITZ, J. D. (1978). *Acta Cryst.* A**34**, 828–829.

SEKIZAKI, M. (1978). Chem. Soc. Jpn Autumn Meet., Abstract 1C6.

SCHOMAKER, V. & TRUEBLOOD, K. N. (1968). *Acta Cryst.* B**24**, 63–76.

SHANNON, R. D. & PREWITT, C. T. (1969). *Acta Cryst.* B**25**, 925–946.

SORAI, M., ENSLING, J. & GÜTLICH, P. (1976). *Chem. Phys.* **18**, 199–209.

SORAI, M., ENSLING, J., HASSELBACH, K. M. & GÜTLICH, P. (1977). *Chem. Phys.* **20**, 197–207.

SORAI, M. & SEKI, S. (1974). *J. Phys. Chem. Solids*, **35**, 555–570.

STEWART, R. F., DAVIDSON, E. R. & SIMPSON, W. T. (1965). *J. Chem. Phys.* **42**, 3175–3187.

TAKEMOTO, J. H. & HUTCHINSON, B. (1973). *Inorg. Chem.* **12**, 705–708.

YANG, Y., BECKER, P. & COPPENS, P. (1979). To be published.

Acta Cryst. (1980). B**36**, 287–292

The Structure of Sodium 3α,7α,12α-Trihydroxy-5β-cholan-24-oate Monohydrate (Sodium Cholate Monohydrate)

BY R. E. COBBLEDICK AND F. W. B. EINSTEIN*

Department of Chemistry, Simon Fraser University, Burnaby, British Columbia, Canada V5A 1S6

(*Received* 18 *April* 1979; *accepted* 7 *September* 1979)

Abstract

The structure of sodium cholate monohydrate, $C_{24}H_{39}O_5^-.Na^+.H_2O$, has been determined with three-dimensional X-ray diffractometer data and refined by full-matrix least-squares calculations to a final R of 0·059 for 1579 observed reflexions. The crystals are monoclinic with space group $P2_1$, $Z = 2$, and unit-cell dimensions $a = 12{\cdot}197\ (7)$, $b = 8{\cdot}214\ (4)$, $c = 12{\cdot}559\ (7)$ Å, $\beta = 108{\cdot}07\ (4)°$. The cholate ions are hydrogen bonded to form spirals parallel to the b axis and further hydrogen bonded across the ends of molecules to give a sandwich sheet structure. The Na ions and the disordered water molecules lie within the polar interior of the sandwich and are involved in ionic and hydrogen bonding. Each Na ion is in contact with five O atoms [Na···O ranging from 2·344 (5)–2·509 (5) Å].

* To whom correspondence should be addressed.

0567-7408/80/020287-06$01.00